JACC: CLINICAL ELECTROPHYSIOLOGY VOL. ■, NO. ■, 2019

Noninvasive Mapping of Premature Ventricular Contractions by Merging Magnetocardiography and Computed Tomography

Satoshi Aita, MD,[a,*] Kuniomi Ogata, MEng,[c,*] Kentaro Yoshida, MD,[a,b] Takeshi Inaba, RDCS,[a] Hisanori Kosuge, MD,[a,d] Takeshi Machino, MD,[a] Yasuaki Tsumagari, MD,[a] Ai Hattori, MD,[a] Yoko Ito, MD,[a] Yuki Komatsu, MD,[a] Kensuke Sekihara, PhD,[e] Hitoshi Horigome, MD,[f] Kazutaka Aonuma, MD,[a] Akihiko Nogami, MD,[a] Akihiko Kandori, PhD,[c,†] Masaki Ieda, MD[a,†]

ABSTRACT

OBJECTIVES This study aimed to develop a novel premature ventricular contraction (PVC) mapping method to predict PVC origins in whole ventricles by merging a magnetocardiography (MCG) image with a cardiac computed tomography (CT) image.

BACKGROUND MCG can noninvasively discriminate PVCs originating from the aortic sinus cusp from those originating from the right ventricular outflow tract.

METHODS This study was composed of 22 candidates referred for catheter ablation of idiopathic PVCs. MCG and CT were performed the same day before ablation. Estimated origins by MCG-CT imaging using the recursive null steering spatial filter algorithm were compared with origins determined by electroanatomic mapping (CARTO, Biosense Webster, Inc., Diamond Bar, California) during the ablation procedure. Radiopaque acrylic markers for the CT scan and coil markers generating a weak magnetic field during MCG measurements were used as reference markers to merge the 2 images 3-dimensionally.

RESULTS PVC origins were determined by endocardial and epicardial mapping and ablation results in 18 (86%) patients (right ventricular outflow tract in 10 patients, aortic sinus cusp in 2 patients, interventricular septum in 1 patient, near His bundle in 1 patient, right ventricular free wall in 1 patient, and left ventricular free wall in 3 patients). Estimated origins by MCG-CT imaging matched the origins determined during the procedure in 94% (17 of 18) of patients, whereas the electrocardiography algorithms were accurate in only 56% (10 of 18). Discrimination of an epicardium versus an endocardium or right- versus left-sided septum was successful in 3 of 4 patients (75%).

CONCLUSIONS The diagnostic accuracy of noninvasive MCG-CT mapping was high enough to allow clinical use to predict the site of PVC origins in the whole ventricles. (J Am Coll Cardiol EP 2019;■:■–■) © 2019 The Authors. Published by Elsevier on behalf of the American College of Cardiology Foundation. This is an open access article under the CC BY-NC-ND license (http://creativecommons.org/licenses/by-nc-nd/4.0/).

From the [a]Department of Cardiology, University of Tsukuba, Tsukuba, Japan; [b]Department of Cardiology, Ibaraki Prefectural Central Hospital, Kasama, Japan; [c]Research and Development Group, Hitachi Ltd., Kokubunji, Japan; [d]Tsukuba Advanced Imaging Center, Tsukuba, Japan; [e]Signal Analysis Inc., Hachioji, Japan; and the [f]Department of Pediatrics, University of Tsukuba, Tsukuba, Japan. *Drs. Aita and Ogata contributed equally to this work and are joint first authors. †Drs. Kandori and Ieda contributed equally to this work and are joint senior authors. This work was supported by JPS KAKENHI grant number JP17K09484. Dr. Aonuma has received a research grant from Hitachi, Ltd. Dr. Nogami has received honoraria from Abbott and an endowment from Medtronic and Johnson and Johnson. Mr. Ogata holds the patent JP6393173B, position estimation method, and position estimation system. Dr. Kandori holds the patent JP6393173B, positional estimation method and positional estimation system. All other authors have reported that they have no relationships relevant to the contents of this paper to disclose.

The authors attest they are in compliance with human studies committees and animal welfare regulations of the authors' institutions and Food and Drug Administration guidelines, including patient consent where appropriate. For more information, visit the *JACC: Clinical Electrophysiology* author instructions page.

Manuscript received January 31, 2019; revised manuscript received May 14, 2019, accepted June 19, 2019.

ABBREVIATIONS AND ACRONYMS

3-D = 3-dimensional

CT = computed tomography

ECG = electrocardiography

ECGi = electrocardiographic imaging

LV = left ventricular

MCG = magnetocardiography

PVC = premature ventricular contraction

RENS = recursive null steering

RFCA = radiofrequency catheter ablation

RVOT = right ventricular outflow tract

Radiofrequency catheter ablation (RFCA) for premature ventricular contractions (PVCs) is an established treatment option to eliminate patient symptoms and prevent PVC-induced cardiomyopathy and heart failure (1). Although technologies such as 3-dimensional (3-D) mapping, irrigated-tip ablation catheters, and contact force monitoring help operators to map and ablate PVCs, procedural complexity, efficacy, and safety still depend on the location of the arrhythmia origin (2). It is especially difficult to eliminate PVCs with an origin near the His-bundle region or in the left ventricular (LV) summit, the intramural layer, or the epicardial aspect. Electrocardiography (ECG) algorithms can identify the area of origin of ventricular arrhythmias, but their spatial resolution is fundamentally low and their diagnostic accuracy can be impaired by the patient's physical characteristics (e.g., obesity and cardiac rotation and offsets of ECG lead placement) (3). Although the utility of magnetocardiography (MCG) to discriminate PVCs originating from the right ventricular outflow tract (RVOT) from those originating from the aortic sinus cusps was previously reported from our center (4,5), this system did not allow mapping of the whole right and left ventricles and identification by the absolute location (coordinates) of the origins. To overcome these limitations and increase the clinical utility of the MCG system for arrhythmia treatments, we developed a custom-made technology to merge MCG images with 3-D computed tomography (CT) images. The aim of this prospective study was to validate this method by comparing the estimated PVC origin on the MCG-CT merged images with that on the map depicted on a 3-D mapping system during catheter ablation.

METHODS

STUDY POPULATION. Twenty-two consecutive patients with PVCs refractory to antiarrhythmic drugs referred for catheter ablation in our hospital between March 2017 and February 2018 were prospectively included in this study. All except 2 patients with coronary artery disease were free of any structural heart disease. The study protocol was approved by the local Institutional Review Board, and all patients provided their informed written consent.

MCG AND CT. MCG can noninvasively measure the weak magnetic field generated by the human heart. The electric current distributions in the heart are estimated from the magnetic field. A superconducting quantum interference device magnetometer is used as the magnetic sensor in MCG. Because the permeability of the human body is constant, detection of the heart's magnetic field is barely affected by other organs around the heart such as fat, bone, and lungs (6–8).

The entire study protocol is outlined in **Figure 1** and the **Central Illustration**. CT examinations were performed 1 week before catheter ablation with a 320-row CT scanner (Aquilion ONE GENESIS Edition, Canon Medical Systems, Otawara, Japan). Just before the CT scan, 5 custom-made radiopaque spherical markers fabricated with acryl and fixed on an L-shaped board were placed on the patients' chests to determine their 3-D location relative to the heart (**Figure 1A**). The parameters for CT imaging were prospective ECG-gated acquisitions, tube potential of 120 kVp, and detector configuration of 320 × 0.5 mm. Scanning was initiated after a threshold of 150 Hounsfield units was reached in the ascending aorta. The CT images were reconstructed at a 0.5-mm slice thickness in the diastolic phase (basically 75% to 77%) of the R-R interval. The CT Digital Imaging and Communications in Medicine images were viewed and edited with Expert INTAGE (CYBERNET SYSTEMS CO., Tokyo, Japan).

Just after the CT scan, the patient was moved to the magnetically shielded room to undergo MCG recording. MCG methodology has been described in detail previously (4,5,9,10). An MCG system (MC-6400, Hitachi High-Technologies Corporation, Tokyo, Japan) with 64 magnetic sensors was used to measure the MCG signal and the magnetic field signal generated from the marker coils. The magnetic sensors were in an 8 × 8 matrix with a pitch of 25 mm and a measurement area of 175 × 175 mm. The MCG signals from each patient were recorded in the resting state in the anteroposterior direction for 2 min at a sampling rate of 1 kHz. The MCG signals were passed through a 0.1- to 50-Hz band-pass filter and a 50-Hz power line noise filter. As during CT scanning, the patients' arms were toward their head during MCG recording. Before MCG recording for PVCs, triaxial (x-y-z axis) circular marker coils, which were fixed on an L-shaped board as the acrylic markers for the CT scan, were placed at the same position as that during the CT scan (**Figure 1B**). A coil driver applied alternating electric current (40 Hz) to each marker coil. The positions of the marker coils on the patient were estimated from the measured magnetic field signals by using an optimization method (Online Appendix). Then, the coordinates of the coil markers for MCG were merged with those of the acrylic markers for CT (**Figure 1C**). Finally, the MCG signals from the PVCs

FIGURE 1 **Entire Study Protocol (See Text for Details)**

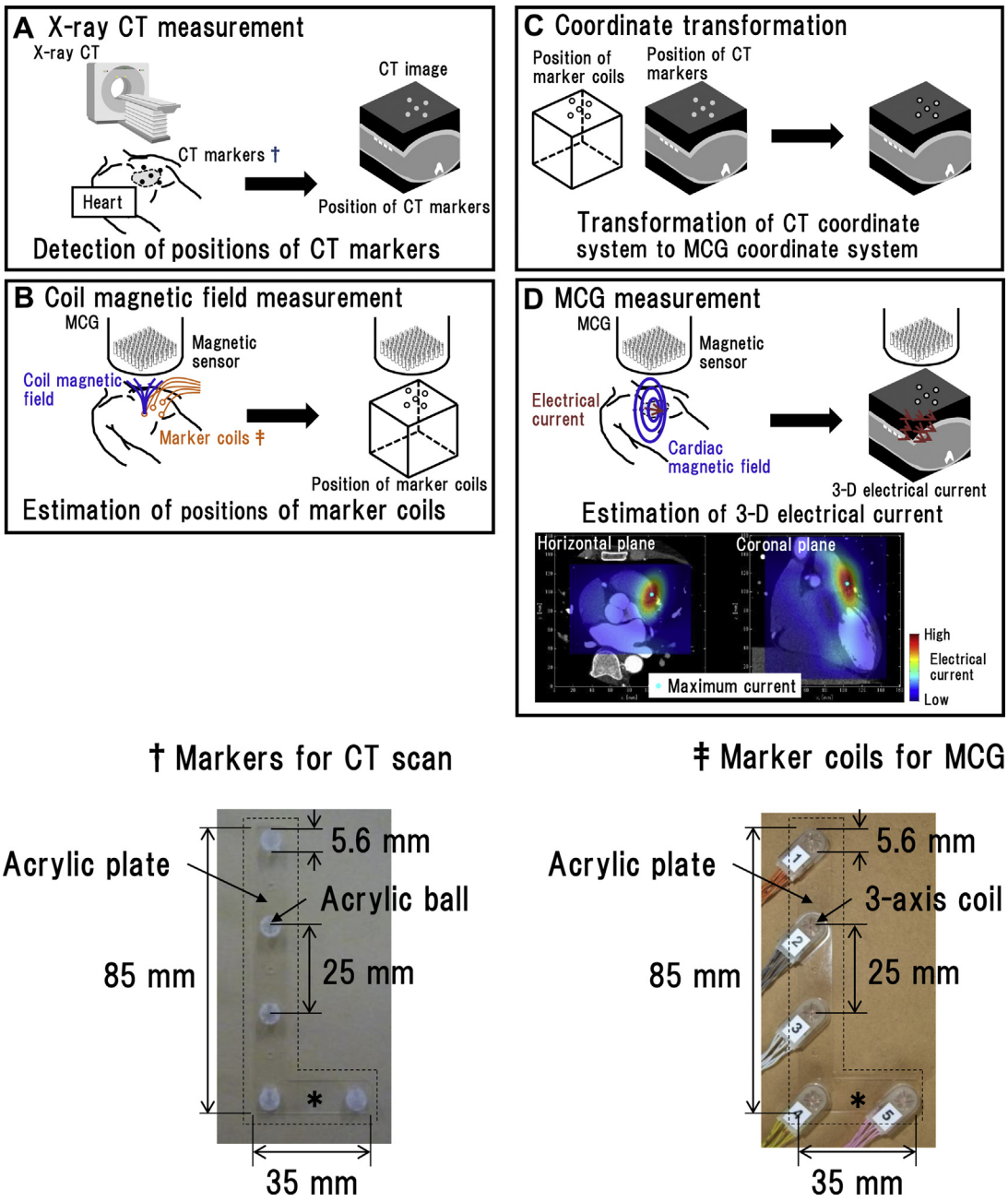

(A) X-ray CT measurement. **(B)** Coil magnetic field measurement. **(C)** Coordinate transformation. **(D)** MCG measurement of PVCs. Acrylic markers for computed tomography imaging **(†)** and marker coils for magnetocardiography recording **(‡)** are shown. CT = computed tomography; MCG = magnetocardiography; PVC = premature ventricular contraction.

were recorded for 2 min, averaged, and then used to reconstruct the 3-D current distribution by applying the recursive null steering (RENS) spatial filter algorithm (**Figure 1D**) (Online Appendix) (11). We developed analysis software in MATLAB (MathWorks, Inc., Natick, Massachusetts) for estimating the position of the marker coils and 3-D current distribution from the MCG measurement.

CENTRAL ILLUSTRATION **Noninvasive Mapping of PVCs by Merging MCG and CT Images**

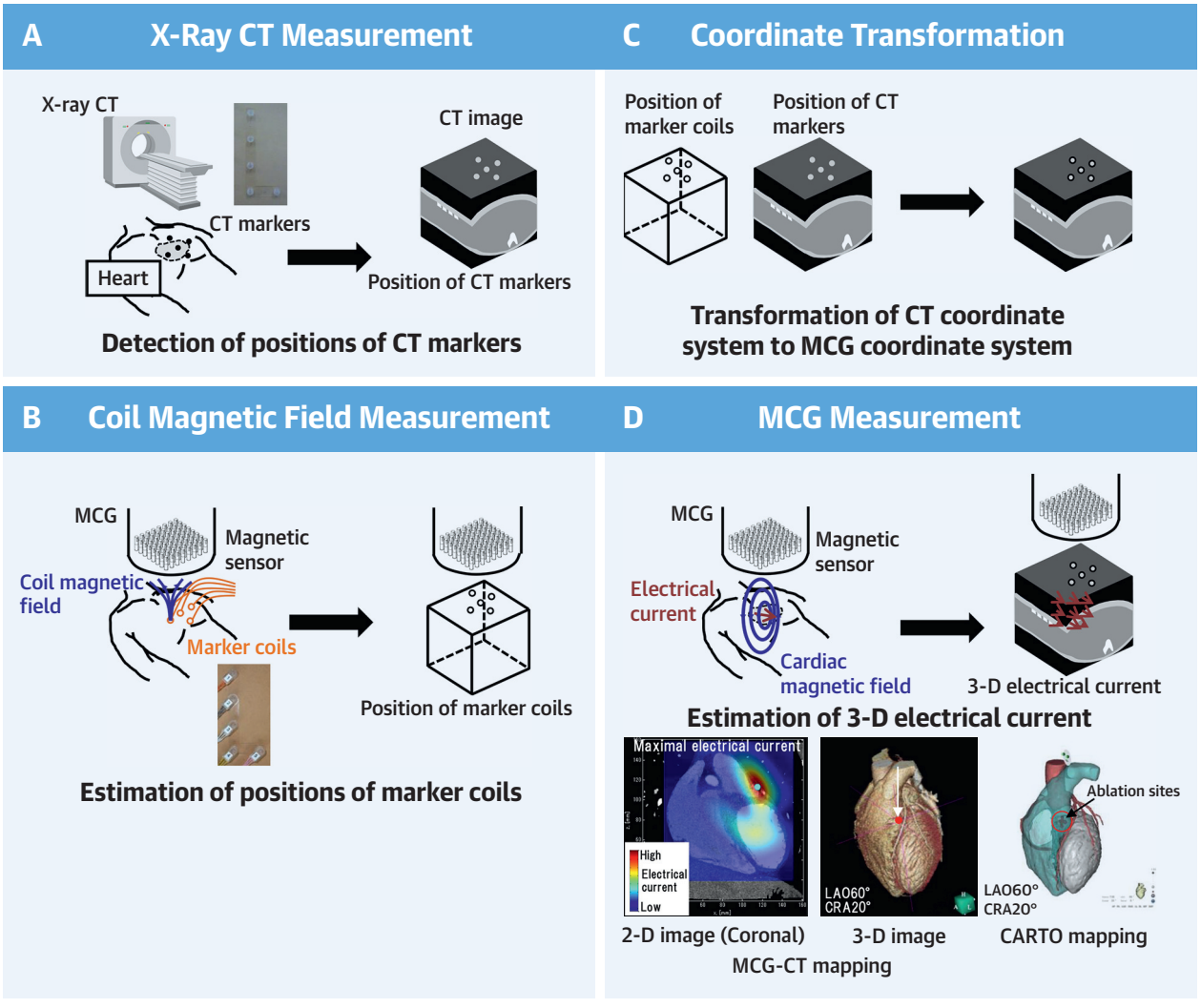

Aita, S. et al. J Am Coll Cardiol EP. 2019;■(■):■-■.

CT = computed tomography; MCG = magnetocardiography; PVC = premature ventricular contraction.

ELECTROPHYSIOLOGICAL STUDY AND CATHETER ABLATION. After informed consent was obtained, electrophysiological study and RFCA were performed. Antiarrhythmic drugs were discontinued for at least 5 half-lives before the procedure. Electrode catheters were placed near the His bundle, coronary sinus, and right ventricular apex. When a target PVC was suspected to originate from the left outflow tract, a 2-F mapping catheter (Japan Lifeline Co., Ltd., Tokyo, Japan) was advanced into the great cardiac vein through the inner lumen of the catheter placed at the coronary sinus (4-mm interelectrode spacing; Inquiry Luma-Cath Fixed Diagnostic Catheter, Abbott, Saint Paul, Minnesota) inserted from the subclavian vein (2). A 7-F quadripolar 3.5-mm-tip open-irrigated ablation catheter (Navistar ThermoCool STSF, Biosense Webster, Inc.) was used for mapping and ablation. A 3-D electroanatomic mapping system (CARTO System Version 4.3.5, Biosense Webster, Inc.) was used to identify the earliest activation site of the target PVC. The radiofrequency energy was delivered at a maximum power of 50 W and a maximum temperature of 42°C. Pace mapping was also performed to search for optimal RFCA

sites. Successful RFCA was defined as complete elimination of the clinical PVC and noninducibility by programmed ventricular stimulation or by a drug provocation test (isoproterenol up to 0.06 μg/kg/min, 20 mg adenosine triphosphate, and 10 mg edrophonium). We defined the site of successful RFCA as the site of PVC origin.

COMPARISON BETWEEN MCG-CT MAP AND ELECTROANATOMIC MAP. The right and left ventricles were divided into 9 and 11 segments, respectively, that were derived from schemas depicted in a previous study (Figure 2) (12). The segment in which a procedure-derived PVC origin was identified was determined based on the electroanatomic map merged with CT imaging by the CARTO system (red closed dots in Figure 2). The operator judged the segment of the procedure-derived origin, and then 2 electrophysiology fellows blinded to the RFCA results independently judged the segment of the MCG-CT-derived origin. These fellows also judged whether the MCG-CT-derived origin was considered endocardial versus epicardial or a left- versus right-sided septum. Discrepancies were resolved by consensus. Although we prospectively included patients in this study, an estimated PVC origin could not be determined before catheter ablation because data analysis took 3 to 4 weeks.

FIGURE 2 Segmentation of the Left and Right Ventricles

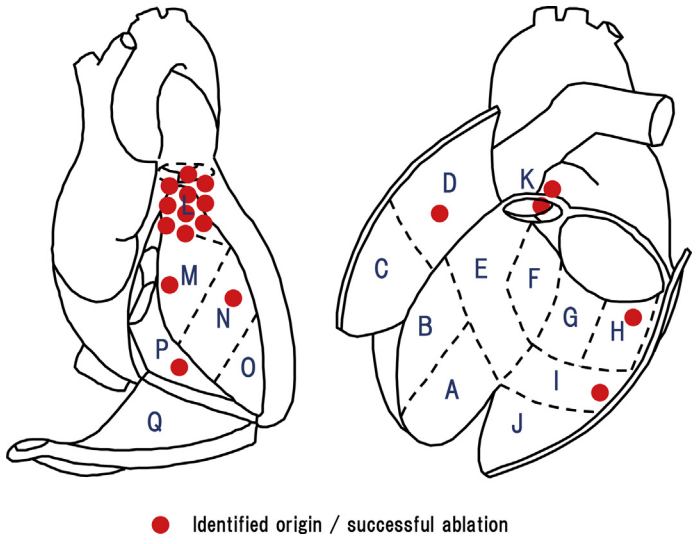

A = inferoapical septum; B = anteroapical septum; C = anteroapical free wall; D = anterobasal free wall; E = anterobasal and mid-septum; F = inferobasal septum; G = inferomedial free wall; H = inferolateral free wall; I = mid-inferior wall; J = inferoapical free wall; K = aortic sinus cusps; L-a = anteroseptal outflow tract; L-m = mid-septal outflow tract; L-p = posteroseptal outflow tract; L-f = outflow tract free wall; M = basal septum; N = mid-septum; O = apical septum; P = inferior wall; Q = lateral free wall.

FOLLOW-UP PROTOCOL. ECG monitoring was continued in all patients from the end of RFCA and throughout hospital stay. After discharge, the patients were followed up at the outpatient clinic, with visits at 1, 3, and 6 months after RFCA, and elimination of the PVCs was confirmed by 12-lead and Holter ECGs recorded at each follow-up visit.

RESULTS

PATIENT CHARACTERISTICS. Eighteen patients were included for further analysis after 4 patients with failed ablation were excluded from the study. Patient details and PVC characteristics are presented in Table 1. The mean patient age was 54 ± 17 years, and 12 (67%) women were included. The mean LV ejection fraction was 65 ± 6%. The QRS morphology of the PVC was a right bundle branch block pattern in 3 (17%) patients and a left bundle branch block pattern in 15 (83%) patients.

PVC ORIGINS AND MCG-CT MAPPING ACCURACY. The distribution of procedure-derived PVC origins in all 18 patients is shown in Table 1 and Figure 2. In 15 cases (68%), spontaneous PVC constantly occurred during the procedure, and we could map the PVC origin by activation mapping. Pace mapping was mainly used in the remaining 7 patients. A correct diagnosis by MCG-CT mapping was obtained in 17 of the 18 patients (94%). Patients with an epicardial origin in the LV anterior wall (Patient #18) (Figure 3), an endocardial origin in the LV lateral wall (Patient #7), and right-sided ventricular septum origin (Patient #3) were correctly diagnosed by MCG-CT mapping. In the 1 patient (Patient #16) with failed diagnosis, the correct origin was the epicardial aspect of the LV posterior wall, whereas the MCG diagnosis was the *endocardial* aspect of the lateral wall (Online Figure 1). Overall, diagnosis of an epicardium versus an endocardium and a right-sided versus left-sided septum was correctly discriminated by MCG-CT mapping in 3 of 4 patients (75%).

ACCURACY OF ECG ALGORITHMS. The ECG algorithms provided by previous studies were also applied to our patients (13–15). They were accurate in 10 of the 18 patients (56%) as shown in Table 1.

REPRESENTATIVE CASES. Patient #18. This 57-year-old man had frequent PVCs originating from the LV outflow tract. A 12-lead ECG of the PVCs is shown in Figure 3A. Figure 3B shows the MCG current maps merged with CT imaging in the horizontal,

TABLE 1 All Patients' Data

Patient #	Age, yrs	Sex	BMI, kg/m²	BNP, pg/ml	PVC Burden, %	EF, %	BBB Type + Axis	Trans. Zone	V1 QRS	Coupl., ms	Analyzed PVCs	Origin (ECG)	Origin (MCG)	Origin (ABL)	Seg.	Area Ablated, cm²	MCG vs. ABL
Successful ablation																	
1	29	F	22.4	19	19.2	65	LBBB IA	V45	rS	451	76	RVOT SEP	RVOT SEP	RVOT SEP	L-m	0.9	Match
2	30	F	18.5	5	5.0	62	LBBB IA	V3	QS	400	1	RVOT POST	RVOT POST	RVOT POST	L-p	1.0	Match
3	67	M	22.3	27	26.7	69	LBBB LAD	V3	QS	411	38	HB	SEP (RV)	SEP (RV)	N	1.9	Match
4	68	F	20.5	13	13.3	73	LBBB SA	V5	QS	465	61	RV INF	RV INF	RV INF	P	1.6	Match
5	69	M	25.7	27	27.0	69	LBBB IA	V34	rS	506	21	ASC	ASC	ASC	K	0.8	Match
6	57	F	29.1	13	12.8	70	LBBB IA	V4	rS	440	1	RVOT POST	RVOT AS	RVOT AS	L-a	1.1	Match
7	80	M	25.6	11	11.0	60	RBBB RAD	V56	RR	471	4	LV LAT	LV LAT (endo.)	LV LAT (endo.)	I	0.9	Match
8	77	F	21.4	18	18.0	65	LBBB IA	V23	qrS	451	38	ASC	ASC	ASC	K	0.9	Match
9	53	F	20.9	42	15.0	62	LBBB IA	V23	rS	408	17	RVOT AS	RVOT AS	RVOT AS	L-a	1.8	Match
10	34	F	22.2	85	33.7	53	LBBB IA	V34	QS	451	38	RVOT FW	RVOT AS	RVOT AS	L-a	1.3	Match
11	36	F	23.0	67	27.0	57	LBBB IA	V34	rS	428	27	RVOT FW	RVOT FW	RVOT FW	L-f	1.2	Match
12	52	M	25.1	12	11.0	68	LBBB IA	V34	rS	627	15	RVOT FW	RVOT POST	RVOT POST	L-p	1.4	Match
13	40	F	21.2	31	17.0	73	LBBB IA	V45	rS	376	81	RVOT FW	RVOT AS	RVOT AS	L-a	1.3	Match
14	43	F	22.7	42	16.8	69	LBBB IA	V34	QS	484	8	RVOT AS	RVOT AS	RVOT AS	L-a	2.5	Match
15	39	F	19.7	12	22.0	67	LBBB IA	V34	rS	455	1	RVOT SEP	RVOT FW	RVOT FW	L-f	1.5	Match
16	79	M	22.9	56	8.0	65	RBBB SA	V56	RR	444	1	LV INF	LV LAT (endo.)	LV POST (epi.)	H	1.1	Mismatch
17	70	F	21.8	10	6.3	64	LBBB LAD	V12	QS	429	15	HB	HB	HB	M	0.7	Match
18	57	M	37.7	58	39.0	56	RBBB IA	< V1	Rs	538	41	ASC	LV ANT (epi.)	LV ANT (epi.)	D	1.0	Match
Failed ablation																	
19	69	F	25.3	35.9	13.7	62	LBBB IA	V3	rS	440	5	RVOT AS	LV ANT (epi.)	NA	NA	NA	NA
20	66	F	25.0	27.0	27.7	45	LBBB IA	V23	qrS	437	26	RVOT SEP	RVOT SEP	NA	NA	NA	NA
21	56	M	21.7	42.7	15.8	73	LBBB LAD	V12	qrS	520	16	RVOT SEP	LV SEP	NA	NA	NA	NA
22	39	F	20.6	48.9	8.0	58	LBBB LAD	V45	rS	556	2	RV LAT	RV SEP	NA	NA	NA	NA

ABL = ablation; ANT = anterior wall; AS = anteroseptal; ASC = aortic sinus cusp; BMI = body mass index; BNP = brain natriuretic peptide; Coupl. = coupling interval; ECG = electrocardiography; EF = left ventricular ejection fraction; endo. = endocardium; epi. = epicardium; F = female; FW = free wall; HB = His bundle; IA = inferior axis; INF = inferior wall; LAD = left axis deviation; LBBB = left bundle branch block; LAT = lateral wall; LV = left ventricle; M = male; MCG = magnetocardiography; NA = not applicable; POST = posterior wall; PVC = premature ventricular contraction; RAD = right axis deviation; RBBB = right bundle branch block; RV = right ventricle; RVOT = right ventricular outflow tract; SA = superior axis; SEP = septum; Seg. = segment; other abbreviations as in Figure 2.

coronal, and sagittal planes where the maximum current during the PVC is shown in red. Figure 3C indicates the coordinates of PVC origin by the crossed lines, and Figure 3D indicates them 3-dimensionally on the CT map. Of note, the left coronary artery on the epicardial aspect (red dashed arrows) was adjacent to the PVC origin (red closed dot). The results from CARTO and fluoroscopic imaging during the ablation procedure are shown in Figure 3E. Based on the recording of the local electrograms (Figure 3F), the great cardiac vein was activated earlier than the LV endocardium and aortic sinus cusps. First, we applied RFCA to the left coronary cusp followed by the LV endocardium (left and

FIGURE 3 Patient #18 With PVCs Originating From the Left Ventricular Epicardium

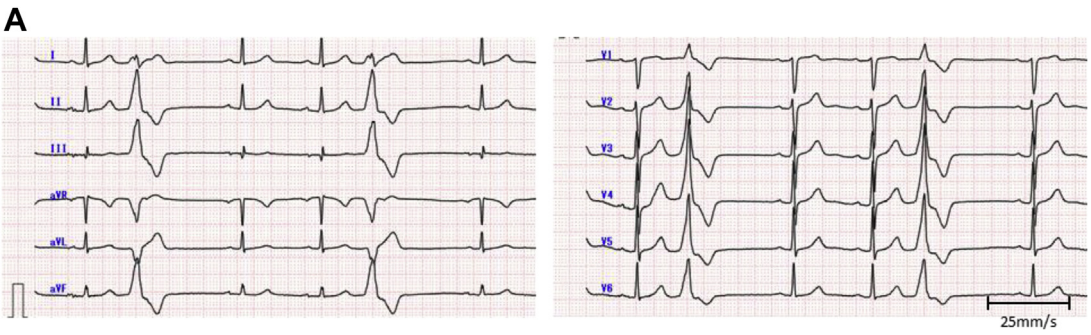

(A) Electrocardiography, **(B)** electrical current maps merged with CT imaging in the horizontal, coronal, and sagittal planes. **(C)** Coordinates of PVC origin shown by the **crossed lines**. **(D)** 3D CT map, **(E)** fluoroscopic imaging and CARTO mapping, and **(F)** intracardiac electrogram in Patient #18 with PVCs originating from the epicardial aspect of the left ventricular anterior wall. The **blue dots in B** correspond to the position of the maximal current amplitude of the 3-D electrical current distribution reconstructed by the RENS filter. These dots were automatically located based on the numerical data by the system. The **yellow dots in E** indicate the successful ablation sites in the great cardiac vein (GCV) (see text for details). ABL = ablation; ASC = aortic sinus cusp; CS = coronary sinus; GCV = great cardiac vein; LAO = left anterior oblique view; LCC = left coronary cusp; LV endo. = left ventricular endocardium; PVC = premature ventricular contraction; RAO = right anterior oblique view.

Continued on the next page

bottom panels of fluoroscopic images in Figure 3E). Transient suppression of the PVCs during the applications was observed, but the PVCs immediately recurred. Next, we advanced the ablation catheter into the great cardiac vein (right panel of fluoroscopic imaging in Figure 3E). Its local activation time preceded QRS onset by 30 ms, and ablation in the vein eliminated the PVCs completely. It was notable that the successful ablation site matched the estimated origin by MCG-CT mapping.

Patient #7. The estimated origin by MCG-CT mapping (red closed dot) was the endocardial lateral wall in the left ventricle (Figures 4A to 4C, Table 1, Online Figure 2). Ablation at the same site on the CARTO map (Figure 4D) successfully eliminated the PVCs. Notably, MCG-CT mapping predicted an endocardial origin but not an epicardial origin in this case.

Patient #2, 10, and 11. Three patients with PVCs originating from the RVOT are shown in Figures 5A to 5C (Table 1, Online Figure 3). The red closed dots in Figures 5A to 5C indicate the estimated origins by MCG-CT mapping, and the ablation sites are shown by red tags on the respective CARTO maps. The posterior site of the RVOT (Figure 5A), anterior site of the RVOT (Figure 5B), and free wall site of the RVOT (Figure 5C) were correctly diagnosed by MCG-CT mapping. The PVCs in these patients were successfully eliminated by ablation.

Patient #16. The mismatch of results is described in detail in Online Figure 1.

FAILED ABLATION. The details of failed ablation are described in Table 1. In Patient #19, MCG-CT mapping estimated the origin in the epicardial aspect of the anterior wall of the left ventricle. Although we tried to ablate it from the great cardiac vein, high impedance did not allow delivery of radiofrequency applications. In Patient #20, MCG-CT mapping estimated the origin in the septal aspect of the RVOT, but the aortic sinus cusp was targeted for ablation. Because the PVC was infrequently observed during the procedure, it was difficult to identify the correct origin. In Patient #21, MCG-CT mapping estimated the origin in the LV septum, but only the right ventricular septum was actually targeted for ablation and the LV septum was not mapped. In Patient #22, MCG-CT mapping estimated the origin in the right ventricular septum. Ablation was applied to the lateral wall of the RV, but it did not eliminate the PVCs.

DISCUSSION

The key observations of the present study are as follows: 1) a novel method to merge the MCG map with the CT image using custom-made markers worked successfully and identified the sites of origin in patients with PVCs originating from both ventricles; 2) accuracy was 94% in patients who had PVCs successfully eliminated by catheter ablation, whereas that of the ECG algorithm was lower as previously reported (16); and 3) from the theoretical and mathematical viewpoints, this technology may have the

FIGURE 3 Continued

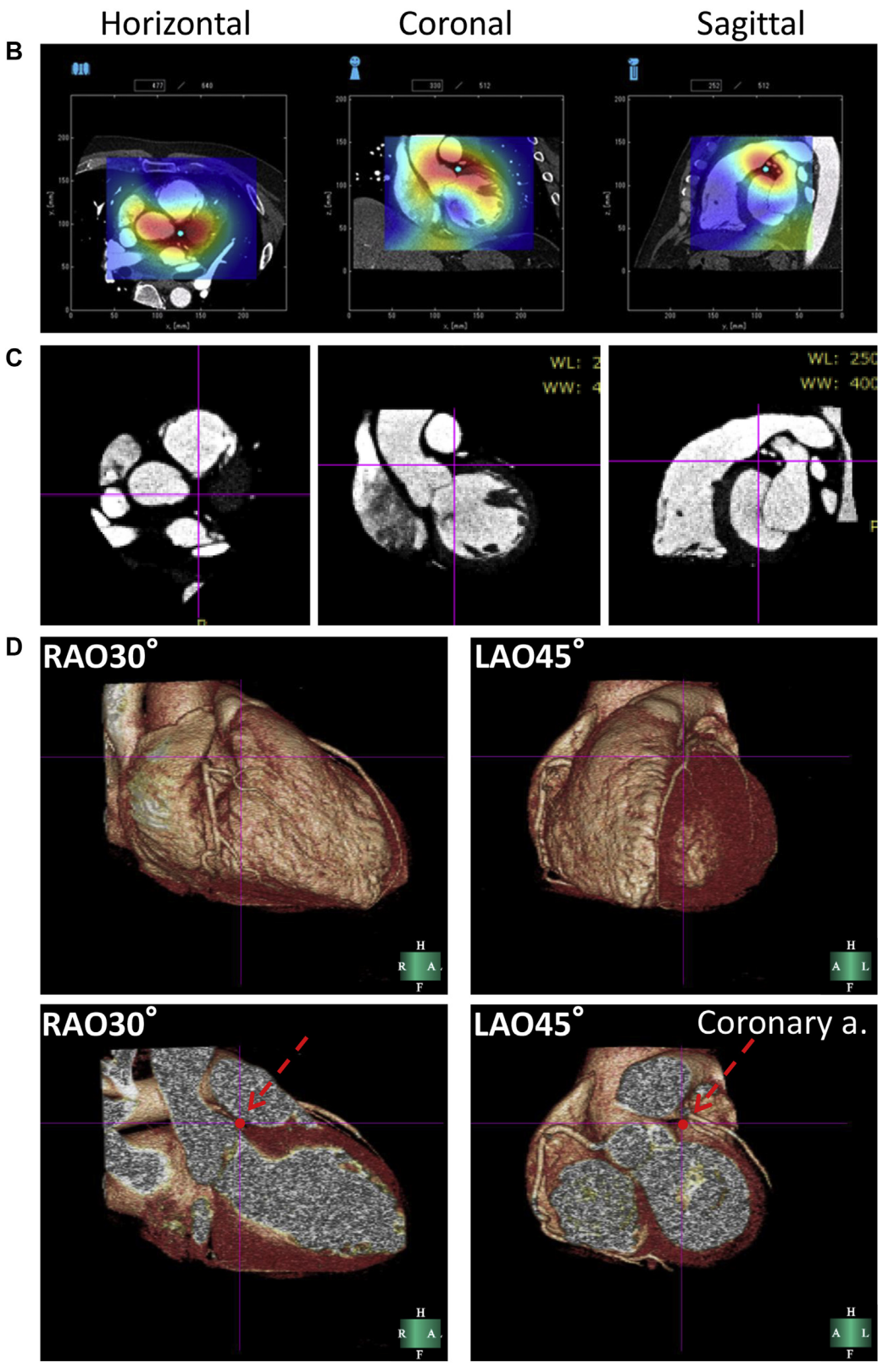

Continued on the next page

FIGURE 3 Continued

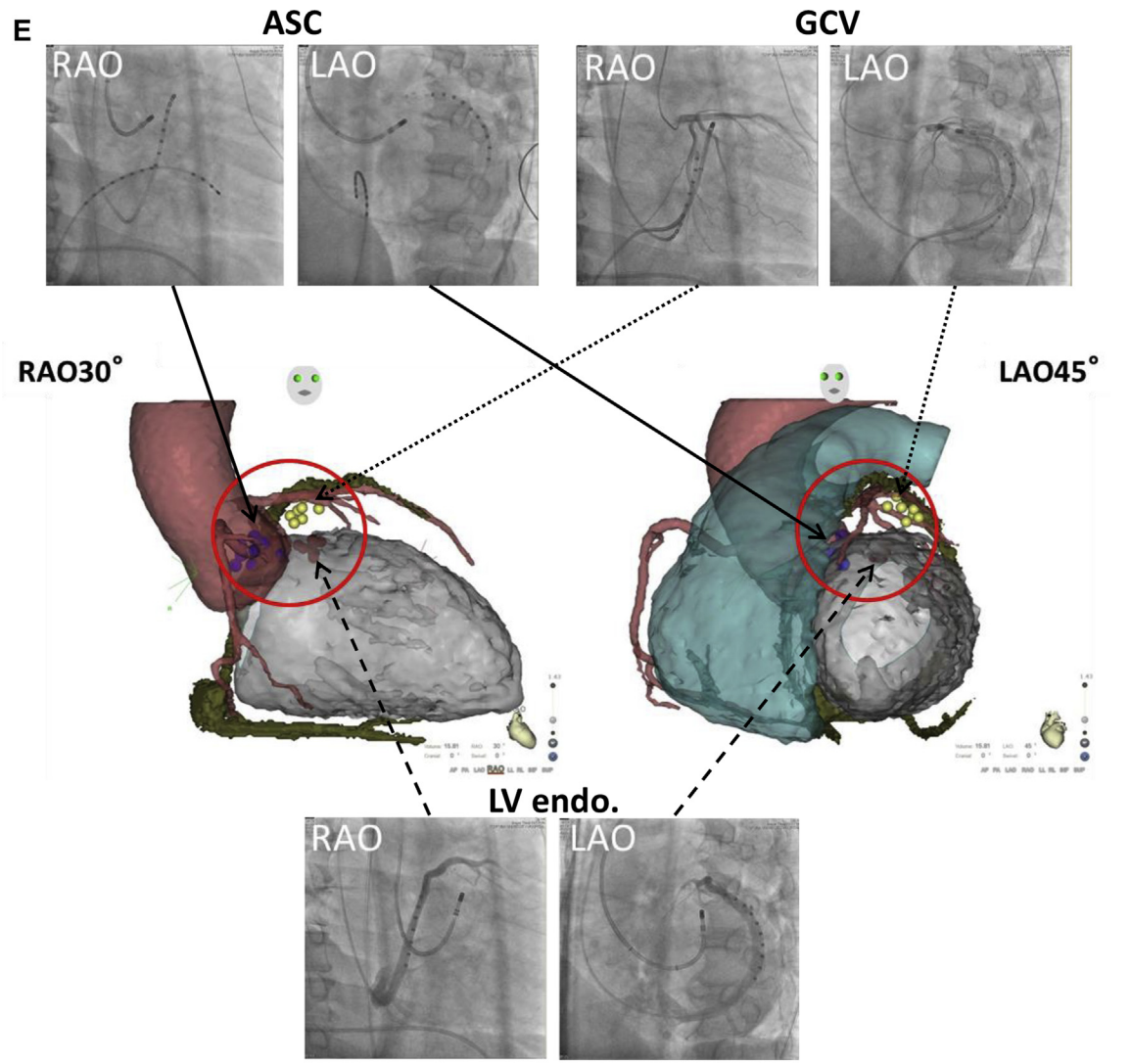

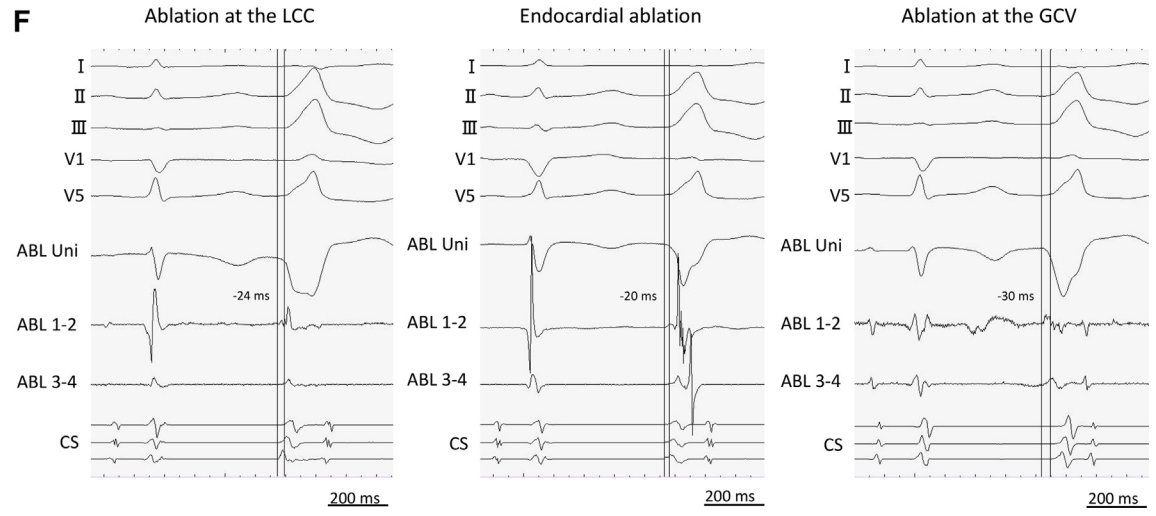

FIGURE 4 **Patient #7 With PVCs Originating From the Left Ventricular Endocardium**

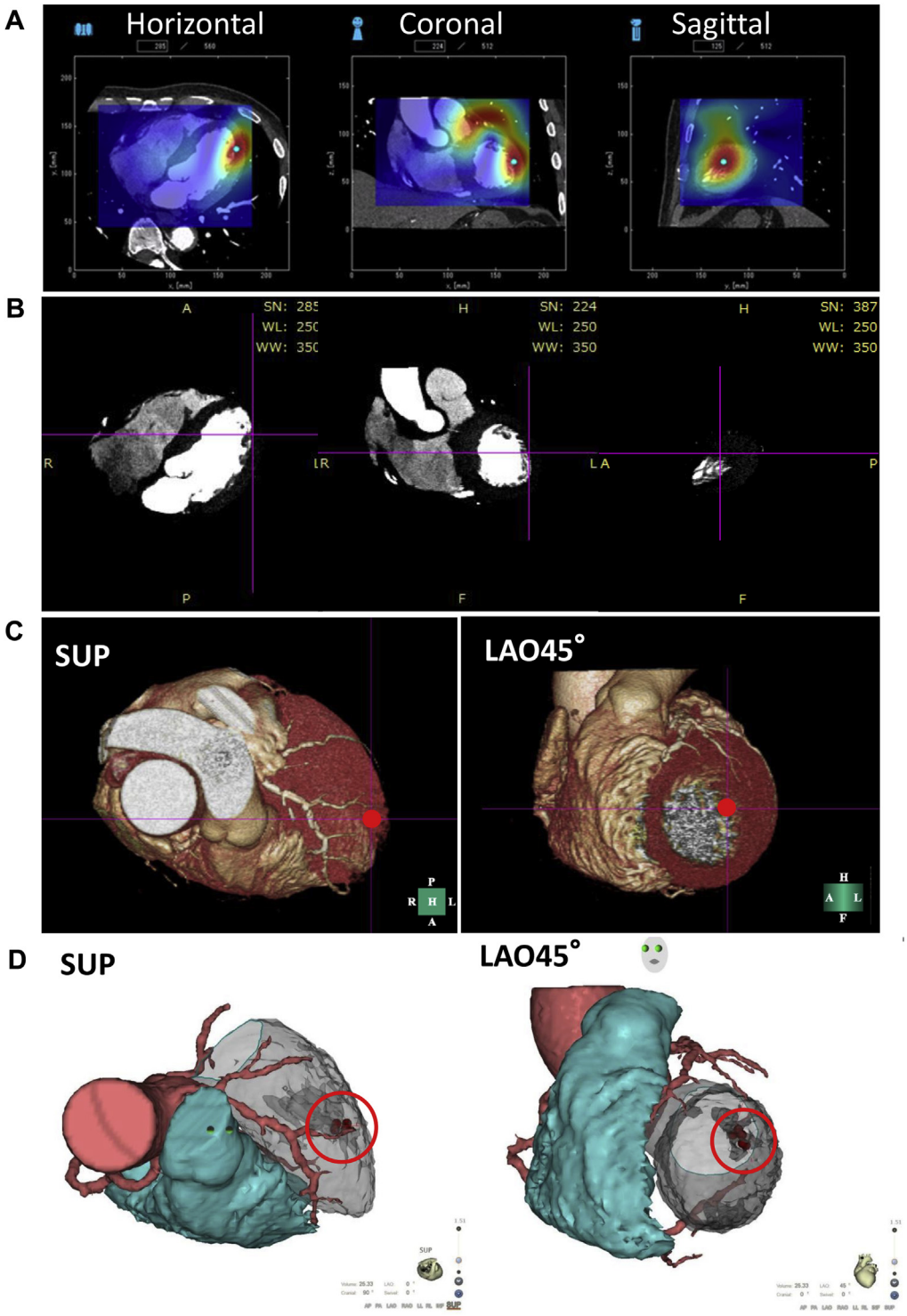

(A) Electrical current maps merged with CT imaging in the horizontal, coronal, and sagittal planes. **(B)** Coordinates of PVC origin shown by the crossed lines. **(C)** 3D CT map and **(D)** CARTO map in Patient #7 with premature ventricular contractions originating from the endocardial side of the lateral wall of the left ventricle (see text for details). LAO = left anterior oblique view; SUP = superior view.

FIGURE 5 **Patients With PVCs Originating From the Right Ventricular Outflow Tract**

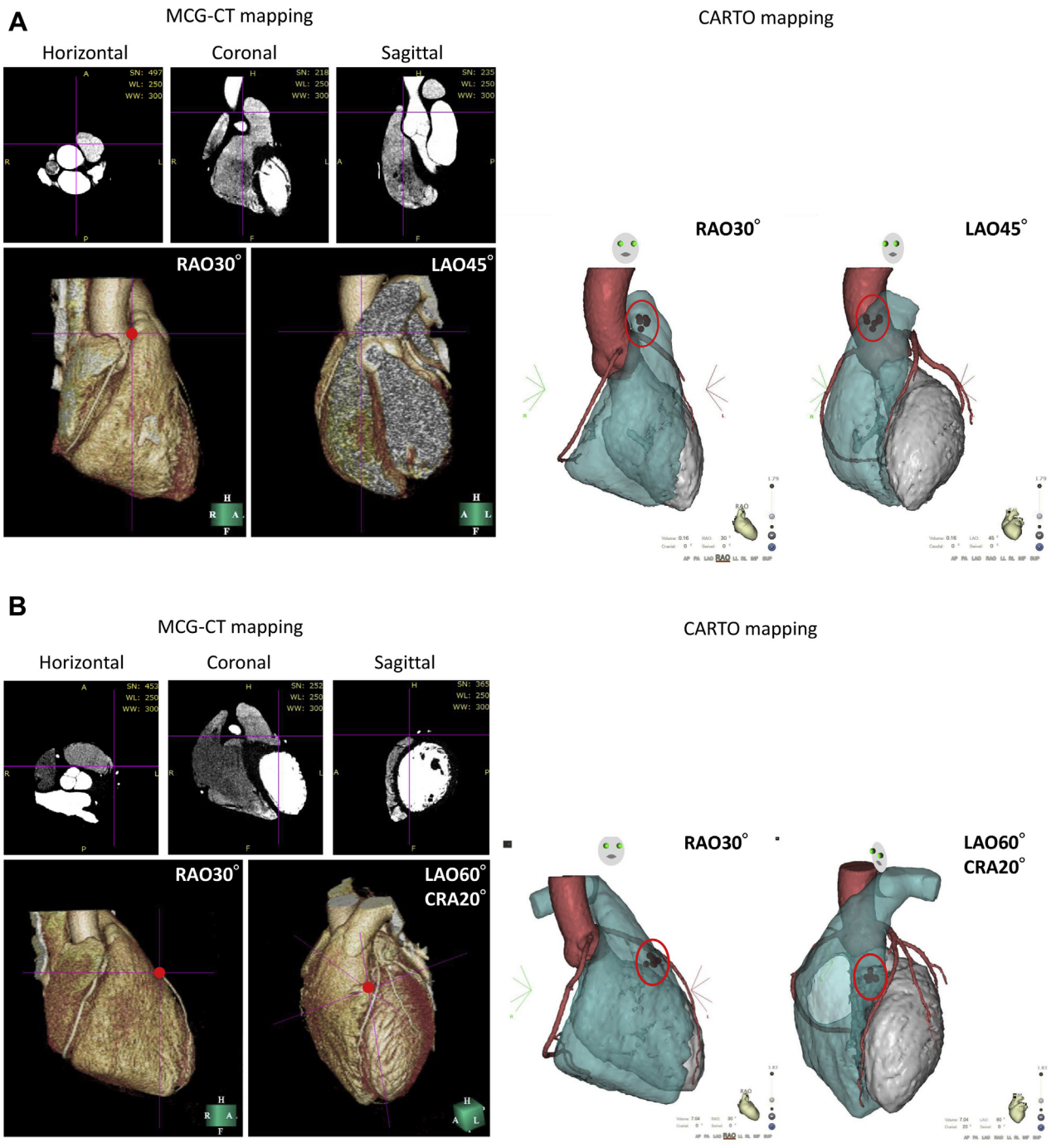

Magnetocardiography–computed tomography (MCG-CT) mapping and CARTO mapping in Patients #2, #10, and #11 with PVCs originating from the right ventricular outflow tract, **(A)** posterior site, **(B)** anterior site, and **(C)** free wall site, respectively (see text for details). CRA = cranial view; LAO = left anterior oblique view; PVC = premature ventricular contraction; RAO = right anterior oblique view.

Continued on the next page

FIGURE 5 Continued

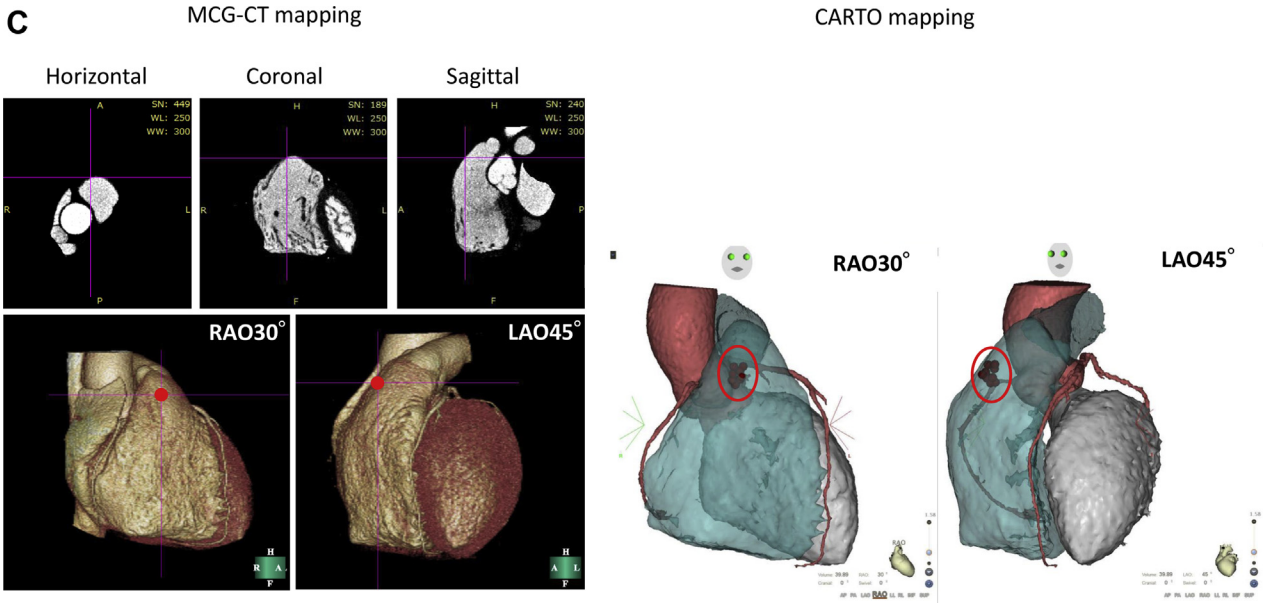

potential to identify transmural distribution of sites of origin (epicardial vs. endocardial origin and right-sided vs. left-sided septal origin). Although this study provides only preliminary results, the findings from a few cases shown in the figures have encouraged us to undertake additional study of more subjects and update the merge function.

Fundamentally, MCG has higher spatial resolution than ECG because the magnetic field is not distorted by flow through tissues such as lungs, bones, and muscles. The RENS spatial filter algorithm can reconstruct a source distribution from bioelectromagnetic data with a spatial resolution considerably higher than that of conventional methods. The robustness of this method to the source correlation was previously validated in our computer simulation and our experiments using auditory-evoked magnetoencephalographic data (11). The present method to 3-dimensionally merge MCG and CT images further enhanced these advantages and the clinical utility of the MCG system in arrhythmia treatments.

MERGING THE MCG MAP WITH THE CT IMAGE. Although our mathematical evaluation of the MCG-CT merged method calculated its error to be within 3 mm, its accuracy may be impaired by several factors in humans such as effects caused by the respiratory phase or cardiac cycle (systole or diastole), volume status, PVC coupling intervals, number of PVCs analyzed and averaged, and the distance between the MCG sensors and PVC origin. However, most of these negative factors can be overcome. The respiratory effect may be minimized by performing CT scanning and CARTO mapping during the expiratory phase. The end-diastolic phase was selected throughout the CT scan, MCG recording, and CARTO mapping. The volume status was consistent throughout the measurements because CT and MCG mapping were consecutively performed within a few hours of each other on the same day, and all measurements and treatment were performed in the fasting state. Although the PVC coupling intervals varied (Table 1), accuracy did not appear to be affected in this patient series. One possible negative contributor is the small number of PVCs analyzed or averaged. In the single patient (Patient #16) with failed localization by MCG-CT mapping and with PVCs originating from the LV posterior wall, only 1 PVC was recorded during the MCG measurement. This factor may be associated with a decreased signal-to-noise ratio. Another factor is the longer distance between the MCG sensors and the origin of the PVCs. Importantly, the LV posterior wall is further from the sensors than the RVOT area. This could be 1 reason for failed localization because magnetic signals attenuate in proportion to the distance.

Taken together, overall accuracy was ethically acceptable to conduct a prospective validation cohort in a manner that informs the operator of the

estimated PVC origin *before* catheter ablation. Also, the overall accuracy of the ECG algorithms was lower than that of the MCG method, and, particularly, their accuracy in the subdivision of the PVC region was quite low, supporting the clinical value of MCG over ECG (16).

PREVENTING CORONARY ARTERY INJURY. It is well-known that coronary artery injury can occur as a direct thermal effect of RFCA. Although the right coronary artery and left circumflex artery are likely to suffer from such a complication in the ablation of Wolff-Parkinson-White syndrome and mitral isthmus ablation, the left anterior descending artery on the epicardial aspect is also at risk for thermal injury (17). Although PVCs can potentially be treated by ablation from the coronary sinus and its branches (2), the risk of coronary artery injury should be assessed, ideally by a noninvasive method, before the ablation procedure is performed. In this study, we noticed that the locations of the coronary arteries were helpful as landmarks to recognize the detailed and exact location of sites of origin. Because the coronary arteries were precisely depicted in our CT images without processing such as smoothing, attenuation, and volume reconstruction, they provided important safety information to physicians before the procedure and may be 1 of the advantages of our mapping technology.

PRIOR STUDIES. Noninvasive body surface mapping systems for the detection of PVCs, so-called electrocardiographic imaging (ECGi) (CardioInsight Technologies, Inc., Cleveland, Ohio) (16,18) and a noninvasive epicardial and endocardial electrophysiology system (EP Solutions SA, Yverdon-les-Bains, Switzerland) (19–22), were previously introduced. Jamil-Copley et al. (16) investigated 24 patients with outflow tract PVCs using ECGi (RVOT in 18 patients and LVOT in 6 patients). The accuracy for the discrimination between RVOT versus LVOT was 96%. Wissner et al. (21) reported that in 18 (86%) of 21 patients with PVC/VT, the correct ventricular segment was diagnosed as a result of nonquantitative assessment. Of note, these systems depend not on the original but the mathematically reconstructed unipolar electrograms and apply a method to *project* the location data on the simplified heart torso created from CT images. This may result in decreased accuracy or an error in discriminating endocardial, epicardial, and intramural origins. Our novel method can potentially overcome these limitations by not projecting but simply merging the coordinates of origins determined by MCG mapping on an original 3-D CT image. In fact, our method could potentially allow the accurate diagnosis of epicardial origins and the side (right vs. left) of septal origin. Of note, a very recent study reported negative results of ventricular mapping by the ECGi system, which questions many of the conclusions previously drawn from ECGi mapping. This study directly compared the ECGi map and invasive epicardial contact map, and primary epicardial breakthroughs imaged using both methods resulted in very large mean absolute errors of over 70 mm (23).

STUDY LIMITATIONS. First, the study volume is small. Only 2 epicardial origins and 2 aortic sinus cusp origins were included. However, the wide distribution of origins other than those in the common outflow tracts was helpful in evaluating the accuracy of this system in the whole ventricles.

Although we prospectively included patients in this study, the estimated PVC origin could not be determined before catheter ablation because data analysis took 3 to 4 weeks. Currently, we have established a method to analyze data and reconstruct and merge the 3-D map within a few days and conducted a validation study in which the estimated result is informed to the operators before the ablation procedure.

Although we attempted to minimize negative factors impairing the accuracy of this mapping system, respiratory and cardiac motion should particularly be taken into consideration to maximize the performance of this mapping technology in clinical practice.

This study was not a direct comparison of MCG and technologies such as ECGi; it only investigated the system's ability to detect arrhythmia origin (electrical onset). The ability of this technology in other types of arrhythmias remains to be evaluated in future studies.

A quantitative analysis that can provide the spatial resolution of this mapping system could not be conducted because MCG recording requires a magnetically shielded room, making it difficult to perform during pace mapping. Because our technology was completely custom-made, we could not load MCG-CT data into the commercially developed CARTO mapping system. Errors in merging the electroanatomic map depicted by the ablation catheter and CT imaging (within the CARTOMERGE system, Biosense Webster, Inc.) cannot be ignored in the assessment of this study. We are now conducting a new validation study to allow more accurate merging of the CT, MCG, and

CARTO maps. This upgrade will allow complete quantitative analysis of the accuracy of this MCG-CT mapping method in the near future.

CONCLUSIONS

In this preliminary study, MCG-CT mapping could identify sites of PVC origins in both ventricles noninvasively and semiquantitatively. A validation cohort including more patients and further updates to the system are needed to justify the use of contrast medium and radiation during CT scanning and to clarify whether this technology improves procedural outcomes, procedural efficiency, and the safety of catheter ablation for ventricular arrhythmias.

ADDRESS FOR CORRESPONDENCE: Dr. Kentaro Yoshida, Department of Cardiology, Faculty of Medicine, University of Tsukuba, 1-1-1 Tennodai, Tsukuba 305-8575, Japan. E-mail: kentaroyo@nifty.com.

PERSPECTIVES

COMPETENCY IN MEDICAL KNOWLEDGER: adiofrequency catheter ablation for PVCs has become an established treatment option. However, procedural complexity, efficacy, and safety still depend on the location of the PVC origin. Although electrocardiographic algorithms can identify the area of origin of ventricular arrhythmias, their accuracy is fundamentally limited due to the low spatial resolution. A custom-made technology to merge magnetocardiography images with 3-D computed tomography images could accurately identify sites of PVC origin distributed in the whole ventricles (17 of 18, 94%).

TRANSLATIONAL OUTLOOK: This technology may have the potential to improve procedural outcomes, procedural efficiency, and the safety of catheter ablation for ventricular arrhythmias.

REFERENCES

1. Zhong L, Lee YH, Huang XM, et al. Relative efficacy of catheter ablation vs antiarrhythmic drugs in treating premature ventricular contractions: a single-center retrospective study. Heart Rhythm 2014;11:187–93.

2. Komatsu Y, Nogami A, Shinoda Y, et al. Idiopathic ventricular arrhythmias originating from the vicinity of the communicating vein of cardiac venous systems at the left ventricular summit. Circ Arrhythm Electrophysiol 2018;11:e005386.

3. Anter E, Frankel DS, Marchlinski FE, Dixit S. Effect of electrocardiographic lead placement on localization of outflow tract tachycardias. Heart Rhythm 2012;9:697–703.

4. Inaba T, Nakazawa Y, Yoshida K, et al. Routine clinical heart examinations using SQUID magnetocardiography at University of Tsukuba Hospital. Supercond Sci Technol 2017;30:114003.

5. Ito Y, Shiga K, Yoshida K, et al. Development of a magnetocardiography-based algorithm for discrimination between ventricular arrhythmias originating from the right ventricular outflow tract and those originating from the aortic sinus cusp: a pilot study. Heart Rhythm 2014;11:1605–12.

6. Yamada S, Tsukada K, Miyashita T, Kuga K, Yamaguchi I. Noninvasive, direct visualization of macro-re-entrant circuits by using magnetocardiograms: initiation and persistence of atrial flutter. Europace 2003;5:343–50.

7. Kandori A, Miyashita T, Ogata K, et al. Electrical space-time abnormalities of ventricular depolarization in patients with Brugada syndrome and patients with complete right-bundle branch blocks studied by magnetocardiography. Pacing Clin Electrophysiol 2006;29:15–20.

8. Yamada S, Kandori A. Surface mapping and magneto-electrocardiography. In: Gussak I, Antzelevitch C, editors. Electrical Disease of the Heart. London, UK: Springer, 2013:223–38.

9. Yoshida K, Ogata K, Inaba T, et al. Ability of magnetocardiography to detect regional dominant frequencies of atrial fibrillation. J Arrhythm 2015;31:345–51.

10. Sato Y, Yoshida K, Ogata K, et al. An increase in right atrial magnetic strength is a novel predictor of recurrence of atrial fibrillation after radiofrequency catheter ablation. Circ J 2012;76:1601–8.

11. Kumihashi I, Sekihara K. Array-gain constraint minimum-norm spatial filter with recursively updated gram matrix for biomagnetic source imaging. IEEE Trans Biomed Eng 2010;57:1358–65.

12. Yoshida K, Liu TY, Scott C, et al. The value of defibrillator electrograms for recognition of clinical ventricular tachycardias and for pace mapping of post-infarction ventricular tachycardia. J Am Coll Cardiol 2010;56:969–79.

13. Ito S, Tada H, Naito S, et al. Development and validation of an ECG algorithm for identifying the optimal ablation site for idiopathic ventricular outflow tract tachycardia. J Cardiovasc Electrophysiol 2003;14:1280–6.

14. Dixit S, Gerstenfeld EP, Callans DJ, Marchlinski FE. Electrocardiographic patterns of superior right ventricular outflow tract tachycardias: distinguishing septal and free-wall sites of origin. J Cardiovasc Electrophysiol 2003;14:1–7.

15. Yoshida N, Yamada T, McElderry HT, et al. A novel electrocardiographic criterion for differentiating a left from right ventricular outflow tract tachycardia origin: the V2S/V3R index. J Cardiovasc Electrophysiol 2014;25:747–53.

16. Jamil-Copley S, Bokan R, Kojodjojo P, et al. Noninvasive electrocardiographic mapping to guide ablation of outflow tract ventricular arrhythmias. Heart Rhythm 2014;11:587–94.

17. Kimata A, Igarashi M, Yoshida K, Takeyasu N, Nogami A, Aonuma K. Left anterior descending artery spasm after radiofrequency catheter ablation for ventricular premature contractions originating from the left ventricular outflow tract. HeartRhythm Case Rep 2015;1:103–6.

18. Cakulev I, Sahadevan J, Arruda M, et al. Confirmation of novel noninvasive high-density electrocardiographic mapping with electrophysiology study: implications for therapy. Circ Arrhythm Electrophysiol 2013;6:68–75.

19. Revishvili AS, Wissner E, Lebedev DS, et al. Validation of the mapping accuracy of a novel non-invasive epicardial and endocardial electrophysiology system. Europace 2015;17:1282–8.

20. Wissner E, Saguner AM, Metzner A, et al. Radiofrequency ablation of premature ventricular contractions originating from the aortomitral continuity localized by use of a novel noninvasive epicardial and endocardial electrophysiology system. HeartRhythm Case Rep 2016;2:255–7.

21. Wissner E, Revishvili A, Metzner A, et al. Noninvasive epicardial and endocardial mapping of premature ventricular contractions. Europace 2017;19:843–9.

22. Wang Y, Cuculich PS, Zhang J, et al. Noninvasive electroanatomic mapping of human ventricular arrhythmias with electrocardiographic imaging. Sci Transl Med 2011;3:98ra84.

23. Duchateau J, Sacher F, Pambrun T, et al. Performance and limitations of noninvasive cardiac activation mapping. Heart Rhythm 2019;16:435–42.

KEY WORDS catheter ablation, computed tomography, magnetocardiography, noninvasive mapping, premature ventricular contraction

APPENDIX For supplemental methods and figures, please see the online version of this paper.